Published in final edited form as:
JACC Cardiovasc Imaging. 2012 December ; 5(12): 1253–1262. doi:10.1016/j.jcmg.2012.05.017.

Ultrasound-Mediated Vascular Gene Transfection by Cavitation of Endothelial-Targeted Cationic Microbubbles

Aris Xie, BS[*], **Todd Belcik, RDCS**[*], **Yue Qi, MD**[*], **Terry K. Morgan, MD, PhD**[†], **Shivam A. Champaneri, MD**[‡], **Sarah Taylor, PhD**[‡], **Brian P. Davidson, MD**[*], **Yan Zhao, MS**[*], **Alexander L. Klibanov, PhD**[‡], **Michael A. Kuliszewski, BS**[§], **Howard Leong-Poi, MD**[§], **Azzdine Ammi, PhD**[*], and **Jonathan R. Lindner, MD**[*]

[*]Division of Cardiovascular Medicine, Oregon Health & Science University, Portland, Oregon

[†]Department of Pathology, Oregon Health & Science University, Portland, Oregon

[‡]Cardiovascular Division, University of Virginia, Charlottesville, Virginia

[§]St. Michael's Hospital, Toronto, Ontario, Canada.

Abstract

OBJECTIVES—Ultrasound-mediated gene delivery can be amplified by acoustic disruption of microbubble carriers that undergo cavitation. We hypothesized that endothelial targeting of microbubbles bearing cDNA is feasible and, through optimizing proximity to the vessel wall, increases the efficacy of gene transfection.

BACKGROUND—Contrast ultrasound-mediated gene delivery is a promising approach for site-specific gene therapy, although there are concerns with the reproducibility of this technique and the safety when using high-power ultrasound.

METHODS—Cationic lipid-shelled decafluorobutane microbubbles bearing a targeting moiety were prepared and compared with nontargeted microbubbles. Microbubble targeting efficiency to endothelial adhesion molecules (P-selectin or intercellular adhesion molecule [ICAM]-1) was tested using in vitro flow chamber studies, intravital microscopy of tumor necrosis factor-alpha (TNF-α)–stimulated murine cremaster muscle, and targeted contrast ultrasound imaging of P-selectin in a model of murine limb ischemia. Ultrasound-mediated transfection of luciferase reporter plasmid charge coupled to microbubbles in the post-ischemic hindlimb muscle was assessed by in vivo optical imaging.

RESULTS—Charge coupling of cDNA to the microbubble surface was not influenced by the presence of targeting ligand, and did not alter the cavitation properties of cationic microbubbles. In flow chamber studies, surface conjugation of cDNA did not affect attachment of targeted microbubbles at microvascular shear stresses (0.6 and 1.5 dyne/cm^2). Attachment in vivo was also not affected by cDNA according to intravital microscopy observations of venular adhesion of ICAM-1–targeted microbubbles and by ultrasound molecular imaging of P-selectin–targeted microbubbles in the post-ischemic hindlimb in mice. Transfection at the site of high acoustic pressures (1.0 and 1.8 MPa) was similar for control and P-selectin–targeted microbubbles but was associated with vascular rupture and hemorrhage. At 0.6 MPa, there were no adverse bioeffects, and transfection was 5-fold greater with P-selectin–targeted microbubbles.

Reprint requests and correspondence: Dr. Jonathan R. Lindner, Cardiovascular Division, UHN-62, Oregon Health & Science University, 3181 SW Sam Jackson Park Road, Portland, Oregon 97239. lindnerj@ohsu.edu. .

APPENDIX For a supplementary figure and expanded methods, please see the online version of this paper.

CONCLUSIONS—We conclude that ultrasound-mediated transfection at safe acoustic pressures can be markedly augmented by endothelial juxtaposition.

Keywords

contrast ultrasound; gene delivery; microbubbles

Integration of gene therapy into routine clinical practice patients is predicated on the ability to safely and efficiently deliver genetic material to target tissues in a manner that favorably alters cell phenotype. Ultrasound energy can amplify transfer of genetic material into cells of target tissues in vivo, the extent of which is further increased by the coadministration of ultrasound contrast agents composed of protein- or lipid-stabilized gas microbubbles (1–6). Contrast ultrasound-mediated gene delivery (CUMGD) and transfection appears to be most effective when genetic material is coupled to the contrast agent surface (7,8).

The observation that CUMGD increases extravasation and cellular uptake of cDNA strongly suggests that local bioeffects produced by microbubble cavitation is responsible for increased transfection efficiency (4,8,9). In an ultrasound field, microbubble contrast agents undergo either stable cavitation (volumetric oscillation linearly related to acoustic pressure) or inertial cavitation (high-amplitude nonlinear oscillation and physical disruption). Cavitation produces oscillatory shear, high-pressure microstreaming, and physical stretching of endothelial cells (10,11). These local effects can produce physical and functional changes in adjacent cells, such as microporation (2,8,9,12), enhanced permeability through intercellular junctions (13), and triggering of active cellular uptake of macromolecules (14).

Irrespective of the mechanism(s) responsible for CUMGD, the proximity of the contrast agent to the cell surface is likely to be a critical determinant. In vivo, this translates to proximity to the vascular wall since in most tissues microbubbles possess a rheology similar to erythrocytes and remain entirely within the vascular compartment (15). Accordingly, endothelial targeting of ultrasound contrast agents via surface conjugation of ligands could amplify CUMGD by promoting vascular juxtaposition (16). On the other hand, direct apposition of ultrasound contrast agents to the endothelial surface by targeting may not necessarily convey benefit in tissues such as the heart, brain, or skeletal muscle where the majority of microbubbles during CUMGD are resident within capillaries and small noncapillary microvessels, where bubbles are already in proximity to the vessel boundaries. The aim of this study was to investigate whether it is feasible to target DNA-laden microbubbles to the endothelial surface and to determine the relative benefit of using a vascular-targeted approach in terms of both efficacy and safety of transfection for CUMGD.

METHODS

Microbubble preparation

Lipid-shelled decafluorobutane microbubbles with a neutral charge were prepared by sonication of a gas-saturated aqueous suspension of distearoylphosphatidylcholine (2 mg/ml) and polyoxyethylene-40-stearate (1 mg/ml). Cationic bubbles were prepared by adding distearoyltrimethylammoniumpropane (0.4 mg/ml) to the aqueous suspension. For biotinylated cationic or neutral microbubbles, distearoylphosphatidyl-ethanolamine–polyethyleneglycol-2000 (DSPE-PEG2000) biotin (0.1 mg/ml) was added to the aqueous suspension. Fluorescent labeling for intravital microscopy was performed by adding dioctadecyl-tetramethylindocarbocyanine perchlorate (DiI) or dioctadecyloxacarbocyanine perchlorate (DiO). Targeted microbubbles were prepared by conjugating biotinylated monoclonal antibodies (mAb) to the surface of cationic biotinylated microbubbles via a streptavidin link as previously described (16). Antibodies included rat anti-mouse P-selectin

(RB40.34), intercellular adhesion molecule-1 (ICAM-1) (3E2, BD Pharmingen, San Jose, California), and isotype control mAb (R3-34, BD Pharmingen). Plasmid cDNA was charge coupled to microbubbles by incubation of 50 μg per 10^8 microbubbles for 15 min, which produces near saturation (8), and for targeted microbubbles was performed after mAb conjugation. The mean diameter and concentration of microbubbles was determined by electro-zone analysis (Multisizer III, Beckman Coulter, Fullerton, California). Electric surface potential (zeta potential) for cationic and neutral microbubbles was determined by measurement of their electrophoretic mobility (ZetaPALS, Brookhaven Instruments, Holtsville, New York) in 1 mmol/l KCl at pH 7.4.

Microbubble–plasmid coupling

Quantitation of microbubble-associated cDNA was performed by fluorescent labeling of plasmid (pCMV-GL3, Promega, Madison, Wisconsin) with SYBR-Gold (Invitrogen, Carlsbad, California). Microbubbles were separated from the aqueous suspension and washed by flotation centrifugation. After hyperbaric destruction of microbubbles, the cDNA content was evaluated by measuring fluorescent activity (Gemini XPS, Molecular Devices, Sunnyvale, California) compared with a standard.

Characterization of microbubble cavitation

Saline alone or suspensions of cationic microbubbles (1×10^7 ml^{-1}) with and without cDNA were infused through acoustically transparent tubing (2-mm internal diameter, 0.9 ml/min) and were exposed to ultrasound (1 MHz, 30-cycle pulses at a pulse repetition frequency of 50 Hz) at either 0.5- or 1.0-MPa peak negative acoustic pressure (PNAP) using a single-element transducer (Olympus NDT, Olympus, Tokyo, Japan) and a random waveform generator (RAM-5000, Ritec, Warwick, Rhode Island). A second broadband (10 KHz to 20 MHz) transducer was placed at a 60° angle as a passive cavitation detector and was interfaced with a receiver (RAM-5000, Ritec) and an oscilloscope (44MXi-A, Teledyne LeCroy, Chestnut Ridge, New York). Acoustic response was quantified by both initial signal amplitude and rate of signal decay indicating inertial cavitation.

Flow chamber studies

Streptavidin (0.25 mg/ml) was adsorbed on the surface of the disposable component of an inverted flow chamber (GlycoTech, Gaithersburg, Maryland) and blocked with casein. The flow chamber was mounted on a microscope, and microbubble adhesion to either streptavidin-coated or control (casein only) plates was assessed using 8 different microbubble preparations according to the following variables: biotinylated versus nonbiotinylated, cationic versus neutral, with versus without plasmid cDNA (pCMV-GL3, Promega). Microbubble suspensions (1×10^6 ml^{-1}) were infused for 5 min at a shear rate of 0.6 or 1.5 dyne/cm^2, after which adhesion density was averaged from >10 optical fields. Each of the 32 experimental conditions was performed in triplicate.

Intravital microscopy

To test binding efficiency in vivo, intravital microscopy of the cremaster muscle was performed in 5 C57BL/6 mice 8 to 12 weeks of age 1 h after intrascrotal injection of TNF-α (0.5 μg in 100 μl). The cremaster muscle was prepared for intravital microscopy as previously described (16,17). Microbubble adhesion was tested for 4 separate cationic microbubble preparations according to the following 2 variables: ICAM-1–targeted or nontargeted control microbubbles, presence or absence of plasmid cDNA on the surface. Microbubbles (1×10^7) were injected intravenously, and adhesion was assessed 5 min later by fluorescent microscopy in 20 optical fields (total area: 1 mm^2). Differential labeling of microbubbles with DiI and DiO allowed simultaneous injection of 2 agents at a time.

Contrast ultrasound molecular imaging

Contrast-enhanced ultrasound (CEU) molecular imaging of endothelial activation was performed to further evaluate the effect of gene loading on microbubble adhesion. Unilateral hindlimb ischemia (20-min iliac ligation) and reperfusion was performed in 10 C57BL/6 mice anesthetized with inhaled isoflurane. CEU perfusion imaging was performed to evaluate microvascular blood flow in the proximal hindlimb adductor muscles during arterial ligation and approximately 45 min after reflow. For perfusion imaging, a continuous infusion of microbubbles (1×10^6 min^{-1}) was used. Flow was quantified from the product of microvascular blood volume and flux rate derived from post-destruction time-intensity data acquired using a linear-array transducer and a contrast-specific multipulse technique (Contrast-Pulse Sequencing, Sequoia, Siemens Medical Systems, Mountain View, California) operating at a transmission frequency of 7.0 MHz and a mechanical index (MI) of 0.16 (18). Absolute microvascular blood flow was calculated by normalizing muscle microvascular blood volume to the blood pool and dividing by tissue density (1.06 g/cm^3). Thirty minutes after reflow, or after similar anesthesia time in nonischemic controls, molecular imaging of retained microbubbles was performed. Signal from retained microbubbles was calculated from a high-MI (1.0) image obtained 8 min after intravenous injection, from which signal from freely circulating microbubbles was eliminated by digital subtraction of frames subsequently obtained at a pulsing interval of 10 s (16). P-selectin–targeted microbubbles with or without plasmid were tested in random order.

Targeted gene transfection

Targeted CUMGD was performed in the model of post-ischemic hindlimb skeletal muscle in 42 C57BL/6 mice 10 to 12 weeks of age. For these experiments, both hindlimbs underwent ischemia-reperfusion injury. Thirty minutes after reflow, either nontargeted or P-selectin–targeted cationic microbubbles (2×10^8) combined with a firefly luciferase (*luc2*) reporter plasmid with an SV40 promoter region (pGL4.13, Promega) was infused intravenously over 1 min. The proximal adductor muscles of only the left hindlimb were exposed to ultrasound during the injection and for an additional 9 min. Transducers were placed at a fixed distance (2 cm) from the mid-portion of the muscle using a transverse imaging plane. Ultrasound exposure was performed using harmonic power Doppler imaging (Sonos 7500, Philips Ultrasound, Andover, Massachusetts) at 1.6 MHz, a pulsing interval of 5 s, a pulse repetition frequency of 2.5 kHz, and a MI of 0.6, 1.3, or 2.4. Acoustic pressures at the level of the muscle were measured by a 0.075-mm needle hydrophone (Precision Acoustics, Dorchester, United Kingdom). Animals were recovered and in vivo assessment of transfection was determined by optical imaging of luciferase activity 3 days later. D-luciferin (0.15 mg/g) was administered by intraperitoneal injection. Animals were anesthetized with inhaled isoflurane and placed in an optical imaging system (IVIS Spectrum, Caliper Life Sciences, Hopkinton, Massachusetts). Bioluminescent activity was measured 10 min after luciferin injection with an open emission filter and medium binning. Light activity from regions of interest placed over each proximal hindlimb was quantified by total photon flux (photons/s).

Luciferase mRNA

Luciferase mRNA in muscle tissue was measured by real-time polymerase chain reaction (PCR) in an additional 36 mice receiving either P-selectin–targeted (n = 18) or nontargeted (n = 18) microbubbles (see Online Methods).

Vascular permeability and hemorrhage

In order to assess vascular permeability, intravenous injection of Texas Red–labeled dextran (70,000 molecular weight) was performed immediately before contrast ultrasound in an additional 14 mice. After the 10-min ultrasound exposure, fluorescent intensity in the

ultrasound-exposed and control hindlimbs were measured with the in vivo optical imaging system using a 605-nm excitation wavelength and emission filters of 660 to 780 nm. Spectral unmixing was performed to correct for autofluorescence. Upon completion of imaging, the skin was removed, and the adductor muscles were examined for petechiae, which were graded as 0 (none), 1 (sparse), 2 (moderate), and 3 (severe).

Histology

Three days after CUMGD, muscle tissue from ultrasound-exposed and control hindlimbs was fixed and embedded in paraffin. Immunohisto-chemistry was performed using goat anti-luciferase polyclonal primary antibody (Promega, 1:200 dilution) primary mAb and secondary anti-goat IgG conjugated to horseradish peroxidase reporter (ImmPRESS, Vector Laboratories, Burlingame, California) with 3,3′ diaminobenzidine chromagen (Vector Laboratories) detection. To assess the late bioeffects of microbubble destruction, Masson's trichrome staining was performed from the control and ultrasound-exposed hindlimb tissue from mice 5 days after exposure (n = 2 for each acoustic power).

Statistical analysis

Data were analyzed using RS/1 (Domain Manufacturing Corp., Burlington, Massachusetts). All data are displayed as mean ± SD unless otherwise specified. For normally distributed data, 1-way analysis of variance was performed for normally distributed variables with post hoc testing of individual comparisons with paired or unpaired *t* test as appropriate. Bonferroni correction was applied for multiple comparisons. Gene transfection data were not normally distributed and were compared with a Mann-Whitney test. Values of $p < 0.05$ were considered to be statistically significant.

RESULTS

Microbubble carrier characteristics

There were no significant differences in either mean diameter (range: 2.5 to 3.1 μm) or size distribution between the 4 different microbubble agents tested. The zeta potential for nonbiotinylated microbubbles was significantly greater for cationic compared with neutral microbubbles (+64 ± 5 mV vs. −1 ± 2 mV, $p < 0.001$). When microbubbles were biotinylated through addition of DSPE-PEG-biotin in the shell, there was a significant ($p < 0.05$) negative shift in the zeta potential for both cationic (+56 ± 2 mV) and "neutral" (−13 ± 2 mV) microbubbles, which was presumably attributable to the biotin component (isoelectric point pH = 3.5). Charge coupling of plasmid cDNA to the microbubble surface detected by SYBR-gold labeling (Fig. 1A) occurred only for cationic microbubbles and was not altered by biotinylation despite the small change in zeta potential produced by biotinylation (Fig. 1B). The acoustic response from cationic microbubbles at PNAP of 0.5 and 1.0 MPa, measured by both the initial signal amplitude from cavitation on the first pulse and by the rate of cavitation-related signal decay, was not substantially affected by surface coupling of cDNA (Figs. 1C and 1D).

Influence of cDNA on microbubble targeting

Flow chamber evaluation of microbubble attachment to adsorbed streptavidin was used to evaluate whether charge coupling of cDNA to the surface of targeted microbubbles impaired their adherence to surfaces in flow conditions (Fig. 2A). At shear stresses of 0.6 and 1.5 dyne/cm^2, there was minimal nonspecific attachment of nonbiotinylated microbubbles to streptavidin, irrespective of microbubble surface charge or incubation with plasmid cDNA. Attachment density was high for neutral biotinylated microbubbles and was not altered by incubation with plasmid cDNA, which was anticipated because of the minimal amount of

cDNA that is charge coupled with neutral agent. In the absence of plasmid cDNA, attachment of biotinylated microbubbles was significantly less for cationic versus neutral microbubbles. Interestingly, the deficit in attachment for cationic biotinylated microbubbles was corrected by plasmid cDNA coupling to the microbubble surface. In both shear conditions, nonspecific attachment to plates without streptavidin was minimal (<5 per optical field) for all 8 microbubble preparations.

Intravital microscopy of TNF-α–treated cremaster muscle in mice was used to evaluate whether surface coupling of cDNA interferes with the in vivo vascular adhesion of targeted microbubbles in an inflammatory disease–related model. Fluorescently labeled microbubbles remained entirely intravascular after their intravenous injection and were cleared from the circulation after 5 min. There was minimal attachment of nontargeted cationic microbubbles (Fig. 2B). Targeting microbubbles to ICAM-1 by surface conjugation of anti-mouse ICAM-1 mAb increased microvascular retention, the extent of which was not altered by the presence of plasmid cDNA. Almost all attachment was secondary to venular endothelial attachment.

Noninvasive CEU molecular imaging of endothelial P-selectin in a model of murine hindlimb ischemia-reperfusion injury was performed to further evaluate whether gene loading influences microbubble adhesion. During iliac artery ligation, flow was reduced to 0.04 ± 0.01 ml/min/g and increased to 0.47 ± 0.20 ml/min/g at the completion of molecular imaging 45 min after reflow. Retention of targeted microbubbles on CEU was evaluated after intravenous injection of microbubble preparations performed between 30 and 45 min after release of the arterial ligature. Retention was greater for P-selectin–targeted versus nontargeted microbubbles and was not substantially affected by surface coupling of plasmid cDNA (Fig. 3).

Reporter gene transfection

Targeted CUMGD of firefly luciferase reporter plasmid (pGL4.13) was assessed in post-ischemic hindlimb skeletal muscle. For these experiments, both hindlimbs underwent ischemia-reperfusion injury, and only the left proximal hindlimb was exposed to ultrasound. The PNAP for the 3 CUMGD ultrasound settings (MI 0.6, 1.3, and 2.4) were 0.6, 1.0, and 1.8 MPa, respectively. Gene transfection quantified 3 days later by whole-body in vivo optical imaging of luciferase activity was detected only at the site of ultrasound exposure (Fig. 4). Luciferase activity at the 2 highest acoustic pressure conditions (1.0 and 1.8 MPa) was similar for P-selectin–targeted and nontargeted microbubbles (Fig. 4A). Luciferase activity was lower at an acoustic pressure of 0.6 MPa. At this lower pressure, transfection was significantly greater (approximately 5-fold) and more reproducible for the P-selectin–targeted microbubbles. Similar results were found for luciferase gene expression by real-time PCR, which was no different for the 2 agents at 1.8 MPa but was higher for targeted compared with nontargeted microbubbles at 0.6 MPa (31,152 ± 26,022% vs. 7,090 ± 2,155% relative to GAPDH, $p < 0.05$). Immunohistochemistry showed that the majority of luciferase transfection occurred in microvascular endothelial cells, smooth muscle cells, and surrounding perivascular cells irrespective of acoustic conditions and microbubble preparation (Fig. 4C). Greater transfection for the targeted agent tended to be due to greater noncapillary microvascular endothelial transfection.

Bioeffects of cavitation

Although the 2 highest acoustic pressures (1.0 and 1.8 MPa) produced the greatest luciferase transfection on CUMGD, they were also associated with the presence of adverse bioeffects evidenced by petechial bleeding on gross inspection (Fig. 5A). Petechiae were not observed in any animal exposed to low-pressure (0.6 MPa) ultrasound. Yet vascular permeabilization

in the ultrasound-exposed limb, detected by optical imaging of Texas Red–dextran accumulation in tissue immediately after ultrasound exposure (Fig. 5B), was similar for 0.6 and 1.0 MPa and actually lower at 1.8 MPa. Histology 5 days after ultrasound and microbubble exposure did not find any evidence for fibrosis in the muscle or anterior subcutaneous tissues even after exposure at 1.8 MPa (Fig. 5C).

DISCUSSION

The aim of this study was to test the hypothesis that juxtaposition of cationic microbubble carriers to the vessel wall would increase CUMGD. Our results indicate that when using very high acoustic pressures that also produce adverse bioeffects, endothelial-targeting of microbubbles during CUMGD does not further augment gene transfection. At lower acoustic pressures that did not produce adverse bioeffects, transfection of vascular cells was substantially increased by endothelial targeting, indicating that this is a feasible approach for balancing transfection efficiency and safety for gene therapy in diseases characterized by specific endothelial epitopes.

Part of the novelty of this study was to create cationic microbubbles with a targeting moiety. With regard to microbubble design, the targeting ligand was conjugated at the end of a long PEG spacer that was intended to allow interaction with endothelial cell adhesion molecules despite charge-mediated layering of cDNA on the microbubble surface. Images obtained by fluorescent labeling indicated relatively uniform rather than eccentric (flocculent) coverage of plasmid on the microbubble surface, and that microbubble aggregation that can occur with plasmid-shell coupling was relatively low. Our flow chamber studies indicated that cDNA coupling to the surface of microbubbles did not interfere with targeting, but actually increased attachment for cationic microbubbles. This phenomenon was not because of nonspecific interactions between cDNA and streptavidin plates that were absent in control experiments. Instead, it is likely that the genetic material acted to prevent interactions between the cationic lipid shell and the biotin moiety, potentially “straightening” the PEG brush. In vivo studies using intravital microscopy and CEU molecular imaging showed no effect of surface coupling of cDNA on either ICAM-1 or P-selectin targeting. ICAM-1 was selected in this model rather than P-selectin because the latter is also affected to varying degrees simply by surgical exteriorization of the muscle (17). These experiments confirmed that the presence of cDNA on cationic microbubble carriers does not interfere with ligand-mediated endothelial attachment under microvascular shear conditions.

The ultrasound conditions during CUMGD are important when assessing the relative benefit of targeting. In our experiments, we chose an ultrasound pulsing interval of 5 s. This is approximately half the time required for total microvascular refill for microbubbles in skeletal muscle after a destructive pulse (18,19). This scheme allowed us to destroy all microbubbles transiting through the microcirculation within the ultrasound beam and to test the effects of endothelial juxtaposition without any differences in the cumulative number of targeted versus nontargeted microbubbles undergoing cavitation.

There is clear evidence that vascular events other than overt vascular rupture are responsible for gene transfection with CUMGD (11,14,20). Our aim was to safely amplify gene transfection by targeting cationic microbubble carriers to the vascular endothelium. Our in vivo transfection studies demonstrated successful CUMGD at the site of ultrasound in all animals. CUMGD with high pressure ultrasound (1.0 to 1.8 MPa) resulted in a high amount of transfection. However, there were also cavitation-related microvascular ruptures that have been previously described with high-power ultrasound and large doses of microbubble contrast agents (21). There were also no differences in transfection for targeted versus nontargeted microbubbles at high power. It is likely that violent cavitation at high acoustic

pressures produced large-pressure microstreams and vascular effects conducive to transfection irrespective of microbubble position relative the vascular wall. At 0.6 MPa, there was 5 times greater transfection for targeted versus nontargeted microbubbles, and there were no petechial hemorrhages. Yet, at this pressure vascular permeabilization assessed by Texas Red–labeled dextran accumulation did not appear to be any less than at the higher pressures, indicating that cavitation may increase permeability in the absence of severe vascular damage. We believe that the slightly lower signal for Texas red–labeled dextran accumulation at 1.8 MPa was probably because of early interruption of flow caused by hemorrhagic bioeffects at this pressure. Interestingly, Masson's trichrome staining showed no histological evidence for significant long-term effects from high-power ultrasound despite the presence of petechiae.

Study limitations

First, we assessed the location of gene transfection 3 days after transfection but did not directly evaluate the location of gene delivery. Our previous studies using intravital microscopy have demonstrated mainly endothelial and perivascular deposition (8). Also, we did not evaluate the effects of different ultrasound pulsing intervals or frequencies. As mentioned previously, we chose our pulsing interval in order to provide equipoise for comparing our 2 agents. We also believe that the benefit of cationic microbubble targeting will need to be demonstrated in models of ischemic tissue that is a likely therapeutic target for pro-angiogenic gene therapy.

Supplementary Material

Refer to Web version on PubMed Central for supplementary material.

Acknowledgments

Dr. Davidson is supported by a post-doctoral fellowship grant (T32-HL094294) from the National Institutes of Health (NIH). Dr. Leong-Poi is supported by the Clinician Scientist Award from the Heart and Stroke Foundation of Ontario. Dr. Lindner is supported by grants R01-HL-078610, R01-DK-063508, R01-HL111969, and RC1-HL-100659 from the NIH. Dr. Klibanov is a cofounder and minority stockholder of Targeson, through which his laboratory receives an NIH subcontract, and he has received research funding from Philips Research North America. Dr. Lindner has received a grant from GE Medical Imaging. All other authors have stated that they have no relationships relevant to the contents of this paper to disclose.

ABBREVIATIONS AND ACRONYMS

CEU	contrast-enhanced ultrasound
CUMGD	contrast ultrasound-mediated gene delivery
ICAM	intercellular adhesion molecule
mAb	monoclonal antibody
MI	mechanical index
PNAP	peak negative acoustic pressure

REFERENCES

1. Shohet RV, Chen S, Zhou YT, et al. Echocardiographic destruction of albumin microbubbles directs gene delivery to the myocardium. Circulation. 2000; 101:2554–6. [PubMed: 10840004]
2. Taniyama Y, Tachibana K, Hiraoka K, et al. Local delivery of plasmid DNA into rat carotid artery using ultrasound. Circulation. 2002; 105:1233–9. [PubMed: 11889019]

3. Porter TR, Iversen PL, Li S, Xie F. Interaction of diagnostic ultrasound with synthetic oligonucleotide-labeled perfluorocarbon-exposed sonicated dextrose albumin microbubbles. J Ultrasound Med. 1996; 15:577–84. [PubMed: 8839405]
4. Suzuki J, Ogawa M, Takayama K, et al. Ultrasound-microbubble-mediated intercellular adhesion molecule-1 small interfering ribonucleic acid transfection attenuates neointimal formation after arterial injury in mice. J Am Coll Cardiol. 2010; 55:904–13. [PubMed: 20185042]
5. Leong-Poi H, Kuliszewski MA, Lekas M, et al. Therapeutic arteriogenesis by ultrasound-mediated VEGF165 plasmid gene delivery to chronically ischemic skeletal muscle. Circ Res. 2007; 101:295–303. [PubMed: 17585071]
6. Bekeredjian R, Chen S, Frenkel PA, Grayburn PA, Shohet RV. Ultrasound-targeted microbubble destruction can repeatedly direct highly specific plasmid expression to the heart. Circulation. 2003; 108:1022–6. [PubMed: 12912823]
7. Frenkel PA, Chen S, Thai T, Shohet RV, Grayburn PA. DNA-loaded albumin microbubbles enhance ultrasound-mediated transfection in vitro. Ultrasound Med Biol. 2002; 28:817–22. [PubMed: 12113794]
8. Christiansen JP, French BA, Klibanov AL, Kaul S, Lindner JR. Targeted tissue transfection with ultrasound destruction of plasmid-bearing cationic microbubbles. Ultrasound Med Biol. 2003; 29:1759–67. [PubMed: 14698343]
9. Mehier-Humbert S, Yan F, Frinking P, Schneider M, Guy RH, Bettinger T. Ultrasound-mediated gene delivery: influence of contrast agent on transfection. Bioconjug Chem. 2007; 18:652–62. [PubMed: 17419583]
10. Wu J, Nyborg WL. Ultrasound, cavitation bubbles and their interaction with cells. Adv Drug Deliv Rev. 2008; 60:1103–16. [PubMed: 18468716]
11. van Wamel A, Kooiman K, Emmer M, ten Cate FJ, Versluis M, de Jong N. Ultrasound microbubble induced endothelial cell permeability. J Control Release. 2006; 116:e100–2. [PubMed: 17718938]
12. Duvshani-Eshet M, Baruch L, Kesselman E, Shimoni E, Machluf M. Therapeutic ultrasound-mediated DNA to cell and nucleus: bioeffects revealed by confocal and atomic force microscopy. Gene Ther. 2006; 13:163–72. [PubMed: 16177822]
13. Sheikov N, McDannold N, Vykhodtseva N, Jolesz F, Hynynen K. Cellular mechanisms of the blood-brain barrier opening induced by ultrasound in presence of microbubbles. Ultrasound Med Biol. 2004; 30:979–89. [PubMed: 15313330]
14. Meijering BD, Juffermans LJ, van Wamel A, et al. Ultrasound and microbubble-targeted delivery of macromolecules is regulated by induction of endocytosis and pore formation. Circ Res. 2009; 104:679–87. [PubMed: 19168443]
15. Lindner JR, Song J, Jayaweera AR, Sklenar J, Kaul S. Microvascular rheology of Definity microbubbles after intra-arterial and intravenous administration. J Am Soc Echocardiogr. 2002; 15:396–403. [PubMed: 12019422]
16. Lindner JR, Song J, Christiansen J, Klibanov AL, Xu F, Ley K. Ultrasound assessment of inflammation and renal tissue injury with microbubbles targeted to P-selectin. Circulation. 2001; 104:2107–12. [PubMed: 11673354]
17. Lindner JR, Kahn ML, Coughlin SR, et al. Delayed onset of inflammation in protease-activated receptor-2-deficient mice. J Immunol. 2000; 165:6504–10. [PubMed: 11086091]
18. Behm CZ, Kaufmann BA, Carr C, et al. Molecular imaging of endothelial vascular cell adhesion molecule-1 expression and inflammatory cell recruitment during vasculogenesis and ischemia-mediated arteriogenesis. Circulation. 2008; 117:2902–11. [PubMed: 18506006]
19. Dawson D, Vincent MA, Barrett EJ, et al. Vascular recruitment in skeletal muscle during exercise and hyperinsulinemia assessed by contrast ultrasound. Am J Physiol Endocrinol Metab. 2002; 282:E714–20. [PubMed: 11832377]
20. Teupe C, Richter S, Fisslthaler B, et al. Vascular gene transfer of phosphomimetic endothelial nitric oxide synthase (S1177D) using ultrasound-enhanced destruction of plasmid-loaded microbubbles improves vasoreactivity. Circulation. 2002; 105:1104–9. [PubMed: 11877363]
21. Miller DL, Quddus J. Diagnostic ultrasound activation of contrast agent gas bodies induces capillary rupture in mice. Proc Natl Acad Sci U S A. 2000; 97:10179–84. [PubMed: 10954753]

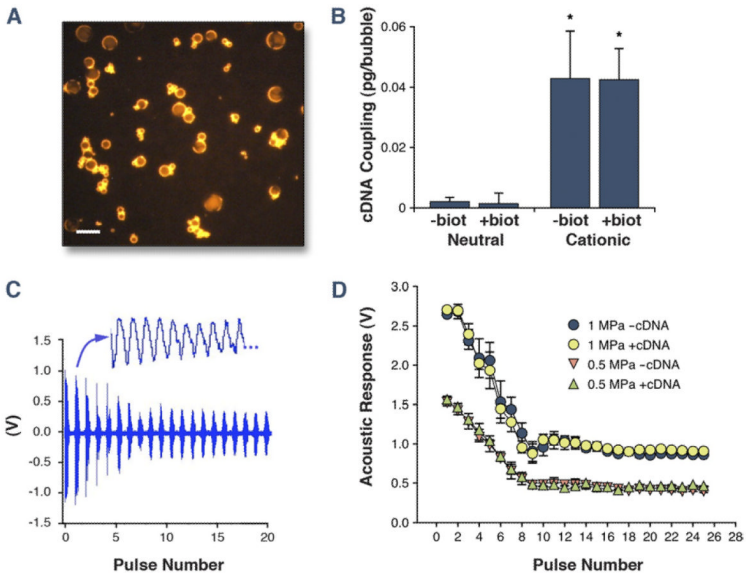

Figure 1. Properties of Lipid Microbubble Carriers

(A) Fluorescent microscopy (excitation filter 530 to 560 nm) of SYBR-gold–labeled plasmid cDNA charge coupled to cationic microbubbles (scale bar = 5 μm). **(B)** Mean ± SD amount of cDNA charge coupled to the surface of different microbubble preparations. Biot = presence of DSPE-PEG-biotin. *$p < 0.01$ versus both neutral preparations. **(C)** Example of an acoustic amplitude response caused by microbubble cavitation during ultrasound exposure at 1 MPa using 30-cycle ultrasound pulses every 20 ms (50 Hz). A portion of the pressure waveform for the second pulse is expanded. **(D)** Mean ± SD amplitude of microbubble response (peak-to-peak) measured by a passive cavitation detector for cationic microbubbles with and without cDNA during sequential 1-MHz ultrasound pulses at 0.5- and 1.0-MPa peak negative acoustic pressure. The eventual stabilization after approximately pulse 10 was not significantly different from that obtained with saline alone (Online Fig. 1).

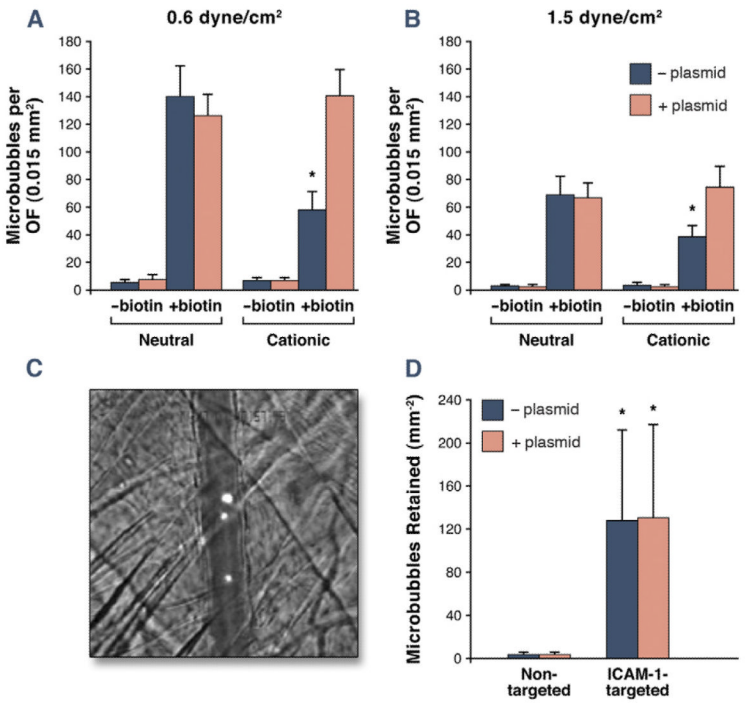

Figure 2. Microbubble Adhesion Efficiency

(A) In vitro microbubble attachment density per optical field (OF) to streptavidin-coated plates in a flow chamber. Data are displayed for shear stresses of 0.6 and 1.5 dyne/cm^2. *p < 0.05 versus both the corresponding neutral biotinylated preparation and the cationic biotinylated preparation with cDNA. **(B)** Illustrative image and quantitative data for in vivo attachment of cationic nontargeted or ICAM-1–targeted microbubbles observed by intravital microscopy in TNF-α–treated cremasteric vessels. The image illustrates retention of DiI-labeled ICAM-1–targeted microbubbles in a venule running vertically across the image (scale bar: 20 μm); *p < 0.05 versus corresponding non-targeted agent.

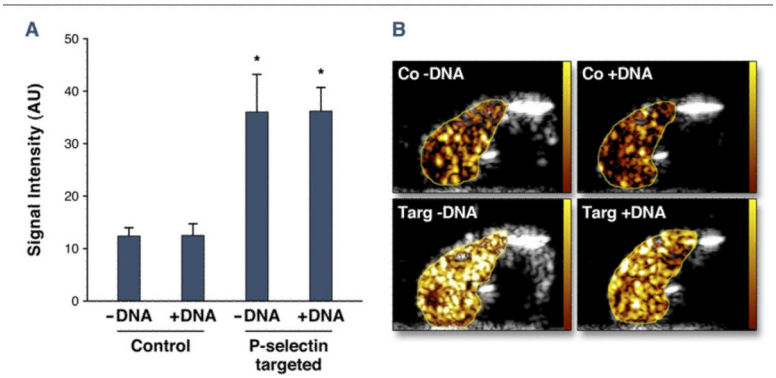

Figure 3. Molecular Imaging of Microbubble Attachment Efficiency

(A) Quantitative acoustic signal intensity (AU) corrected for freely circulating contrast for nontargeted control. *$p < 0.05$ versus corresponding nontargeted agent. **(B)** Examples of contrast-enhanced ultrasound images obtained of the post-ischemic hindlimb skeletal muscle 8 min after intravenous injection for control (Co) or P-selectin–targeted (Targ) microbubbles. Images are color coded (scale at **left**) and subtracted for freely circulating agent.

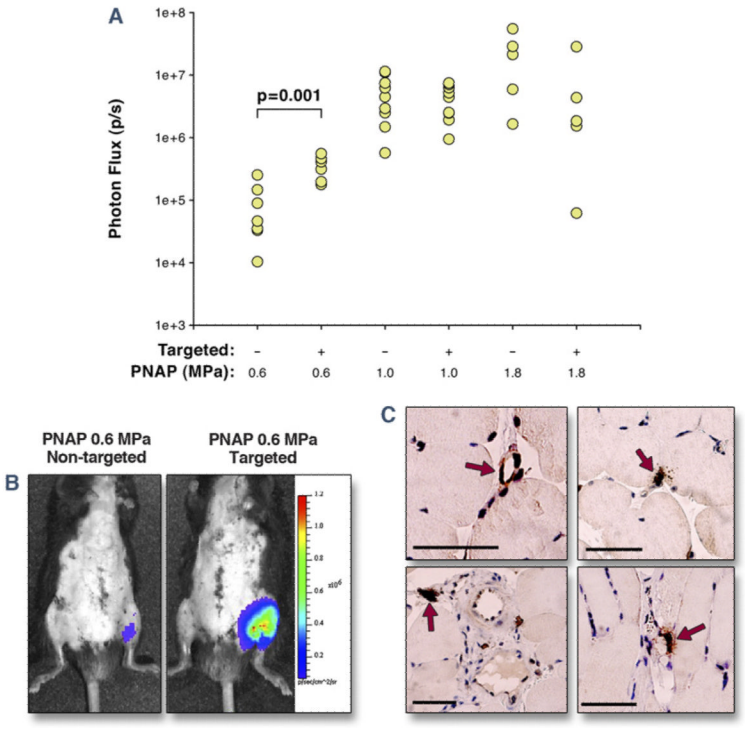

Figure 4. Targeted Transfection of Luciferase Reporter Plasmid

(A) In vivo optical imaging data of luciferase reporter gene transfection 3 days after CUMGD, quantified as photon flux at the site of ultrasound exposure 10 min after intraperitoneal injection of luciferin. PNAP = peak negative acoustic pressure. Transfection was significantly lower at 0.6 MPa compared with 1.0 and 1.8 MPa for both agents. **(B)** Examples illustrating luminescence (color-coded) 3 days after bilateral hindlimb ischemia and intravenous injection of either nontargeted or P-selectin–targeted cDNA-coupled cationic microbubbles during ultrasound at 0.6 MPa. Ventral surface depiliation was performed to reduce light attenuation. **(C)** Immunohistochemistry for luciferase with peroxidase illustrating transfection **(arrows)** of venular and capillary endothelium and perivascular cells. Scale bar = 50 μm.

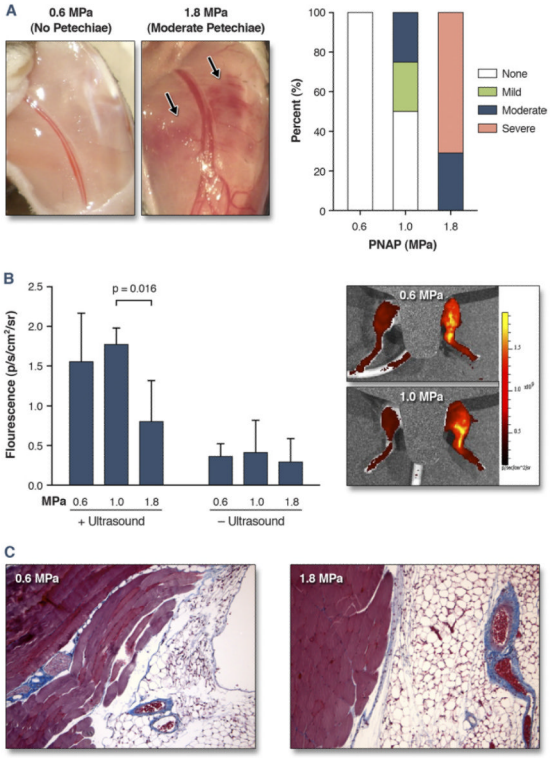

Figure 5. Bioeffects From CUMGD Measured Immediately After Ultrasound Exposure

(A) Examples showing no petechiae or moderate petechiae at the site of ultrasound exposure at peak negative acoustic pressures (PNAP) of 0.6 and 1.8 MPa, respectively, and percentage of animals with each petechia score. **(B)** Quantitative fluorescence for Texas Red–dextran from the ultrasound-exposed and control leg immediately after contrast ultrasound-mediated gene delivery (CUMGD). Examples of in vivo optical imaging (color-coded and superimposed on bright light images) are shown at the **right** with a mid-line shield placed to eliminate bladder signal. **(C)** Masson's trichrome imaging illustrating absence of significant fibrosis **(blue)** other than normal perivascular pattern in tissue exposed to microbubbles and ultrasound at 0.6 or 1.8 MPa.